International Journal of Heat and Mass Transfer 51 (2008) 5269–5278

Contents lists available at ScienceDirect

International Journal of Heat and Mass Transfer

journal homepage: www.elsevier.com/locate/ijhmt

Effects of high subcooling on two-phase spray cooling and critical heat flux

Milan Visaria, Issam Mudawar *

Boiling and Two-Phase Flow Laboratory (BTPFL) and Purdue University International Electronic Cooling Alliance (PUIECA), Mechanical Engineering Building, 585 Purdue Mall, West Lafayette, IN 47907-2088, USA

ARTICLE INFO

Article history:
Received 13 August 2007
Received in revised form 28 February 2008
Available online 3 June 2008

ABSTRACT

Experiments were performed with FC-77 using three full-cone spray nozzles to assess the influence of subcooling on spray performance and critical heat flux (CHF) from a 1.0×1.0 cm^2 test surface. The relatively high boiling point of FC-77 (97 °C at one atmosphere) enabled testing at relatively high levels of subcooling. Increasing the subcooling delayed the onset of boiling but decreased the slope of the nucleate boiling region of the spray boiling curve. The enhancement in CHF was relatively mild at low subcooling and more appreciable at high subcooling. CHF was enhanced by about a 100% when subcooling was increased from 22 to 70 °C, reaching values as high as 349 W/cm^2. The FC-77 data were combined with prior spray CHF data from several studies into a broad CHF database encompassing different nozzles, fluids, flow rates, spray orientations, and subcoolings. The entire CHF database was used to modify the effect of subcooling in a previous CHF correlation that was developed for relatively low subcoolings. The modified correlation shows excellent predictive capability.

1. Introduction

The compounding problem of high-flux heat dissipation from modern electronic and power devices has created an urgent need for effective cooling solutions. Phase change cooling schemes have been at the forefront of choices for such solutions. In particular, solutions that utilize micro-channel flow, jet impingement and sprays appear to attract the most attention from researchers. These schemes offer a variety of thermal and system related benefits but also drawbacks. Micro-channel cooling devices offer compactness, reduced coolant inventory but, potentially, high pressure drop. Jet impingement is especially desirable for cooling very high-flux devices, but may lead to large spatial temperature gradients unless implemented in a carefully configured multi-jet array [1]. Perhaps the most important attribute of spray cooling is the ability to reduce surface temperature gradients compared to both micro-channel and jet impingement cooling schemes.

Spray cooling performance and critical heat flux (CHF) depend on a number of parameters including nozzle type, orifice-to-surface distance, heated surface size, spray orientation relative to surface, Sauter mean droplet diameter, d_{32}, mean droplet velocity, U_m, volumetric flux, Q'', and subcooling. The spray cooling literature includes data for a broad range of fluids including water, dielectric coolants (*e.g.*, FC-72, FC-87 and PF-5052), and refrigerants (*e.g.*, R-113 and R-134a). Not all investigators agree on which spray hydrodynamic parameters should be included in heat transfer correlations. For example, CHF has been effectively correlated in a number of studies to d_{32} and Q'' but not U_m [2–7], others correlated CHF to d_{32} and U_m but not Q'' [8,9].

Influence of distance between the nozzle orifice and the surface has been studied both analytically and experimentally, culminating in a systematic criterion for maximizing CHF. This simple yet powerful criterion consists of setting the orifice-to-surface distance such that the spray impact area just inscribe the square heated surface [6,7,10–12]. Recently, spray cooling research has been focused on using multiple sprays and on improving CHF by surface enhancement [13–16]. Another topic of recent interest has been the effects of spray orientation on spray cooling performance and CHF [11,12,16,17].

One of the more important yet illusive parameters in spray cooling is subcooling. Most databases upon which CHF correlations are based are for fluids that are intended for cooling of electronic and power devices. Aside from dielectric attributes, these coolants are selected based on boiling point. Two-phase coolants must have a boiling point at atmospheric pressure below 85 °C, the upper temperature limit for most commercial electronic devices. This explains the abundance of spray cooling data for FC-72, FC-87 and PF-5052, with boiling points of 56, 30.7 and 50.7 °C, respectively. Because facilities that are used to measure boiling data are typically designed to reject heat to ambient air, subcooling range is limited by the difference between the coolant's boiling point and ambient temperature; about 30 °C for FC-72 down to 5 °C for FC-87. This small subcooling range greatly limits the validity of existing CHF correlations, and a broader range of subcooling must be examined to more accurately capture the influence of this important parameter.

The present greatly broadens the range of subcooling in two-phase spray cooling. To accomplish this goal, experiments were

* Corresponding author. Tel.: +1 765 494 5705; fax: +1 765 494 0539.
E-mail address: mudawar@ecn.purdue.edu (I. Mudawar).

0017-9310/$ - see front matter © 2008 Elsevier Ltd. All rights reserved.
doi:10.1016/j.ijheatmasstransfer.2008.02.045

Nomenclature

c_p	specific heat at constant pressure
d_0	diameter of nozzle orifice
d_{32}	Sauter mean diameter (SMD)
g	gravitational acceleration
h_{fg}	latent heat of vaporization
H	distance of nozzle orifice from test surface
L	length (and width) of square test surface
P	pressure
ΔP	pressure drop across spray nozzle
Q	total volumetric flow rate of spray
$\overline{Q}''$	average volumetric flux across impact area of spray
Q''	local volumetric flux on test surface
q''	heat flux based on total area (L^2) of test surface
q''_m	critical heat flux based on total area (L^2) of test surface
$q''_{m,p}$	local (point-based) critical heat flux at outer edge of spray impact area
Re_{d_0}	Reynolds number based on orifice diameter
T_{in}	liquid temperature at nozzle inlet
T_s	test surface temperature
T_{sat}	saturation temperature based on test chamber pressure
ΔT_{sub}	fluid subcooling at nozzle inlet, $T_{sat} - T_{in}$
U_m	mean droplet velocity
We_{d_0}	Weber number based on orifice diameter
We	Weber number based on Sauter mean diameter and Q'' or $\overline{Q}''$

Greek symbols

η	evaporation efficiency
θ	spray cone angle
μ	viscosity
ρ	density
σ	surface tension

Subscripts

f	liquid
g	vapor
in	nozzle inlet
m	maximum (CHF)
p	point-based (local)
s	test surface
sat	saturation
sub	subcooled

performed with dielectric coolant FC-77, which has a relatively high boiling point of 97 °C. Subcooling was varied from 20.6 to 70 °C for spray flow rates of $Q = 3.33 \times 10^{-6}$–20.4×10^{-6} m^3/s and droplet diameters of $d_{32} = 100$–200 μm. The new broad range of subcooling enabled CHF enhancement by as much as 100%. Aside from the new FC-77 data, prior CHF databases for the afore-mentioned dielectric coolants in addition to limited water data were compiled into a comprehensive database that covers broad variations of fluid, nozzle type, flow rate, droplet size, subcooling, and spray orientation. Using this database, a CHF correlation previously developed by Estes and Mudawar [6] is modified to greatly improve prediction of the subcooling influence.

2. Experimental methods

2.1. Flow loop

The primary purpose of the two-phase flow loop is to deliver FC-77 liquid to the spray nozzle at the desired pressure, flow rate and subcooling. As shown in Fig. 1, liquid coolant is supplied from a large reservoir and passed through a deaeration chamber containing a large immersion heater. The immersion heater is used prior to the spray experiments to deaerate the liquid, as well as during the experiments to heat the coolant to the desired nozzle inlet temperature. Situated beneath the deaeration chamber are two variable-speed, magnetically-coupled centrifugal pumps that are connected in parallel to achieve a broad range of flow rates. The large size and elevation of the reservoir above the pumps helps prime the pumps and maintain stable flow. The pumped fluid first passes through a filter, to remove any entrained impurities, followed by one of two rotameters where flow rate is measured. The fluid then passes through an in-line electric heater followed by an air-cooled heat exchanger. Given the high boiling point of FC-77 of 97 °C, the in-line heater provides additional heating of the coolant in low subcooling experiments. The air-cooled heat exchanger brings the liquid temperature to the desired level of subcooling, especially in high subcooling experiments, before the liquid enters the spray nozzle situated inside the spray chamber. The spent fluid separates inside the spray chamber; liquid drains to the loop's reservoir while vapor rises to a condenser situated above the reservoir.

2.2. Test heater

Fig. 2 shows the constructional details of the test heater used in the present study. The heater is made mostly from oxygen-free copper. Nine 220 W cartridge heaters are inserted into the copper block's underside. The copper block narrows stepwise upwards to expose a 1×1 cm^2 test surface to the spray. This heater design enables safe dissipation of very high-heat fluxes from the test surface. Except for the test surface, all other surfaces of the copper block are insulated with G-7 plastic and fiberglass. Temperature is measured by a type-*K* (Chromel–Alumel) thermocouple embedded 1.27 mm below the test surface. The test surface temperature is determined by assuming 1-D conduction between the thermocouple and the test surface. The heater surface protrudes slightly above the G-7 insulation to prevent liquid accumulation on the test surface. Ref. [10] provides additional details concerning the heater construction and the inference of test surface temperature.

2.3. Operating procedure

Before commencing an experiment, the spray nozzle is connected inside the spray chamber and the spray chamber carefully sealed. The reservoir is then filled with liquid and the entire loop closed to the ambient. Deaeration is achieved by vigorously boiling the coolant inside the deaeration chamber for about 30 min. The condenser's outlet valve is cracked slightly open during the deaeration to release any noncondensible gases to the ambient as the condensed liquid drains back to the reservoir. The pumps are then turned on and deaeration allowed to continue an additional 15 min while the coolant circulated through the loop. The condenser valve is finally closed to isolate the loop from the ambient. Pump speed is then adjusted to the required flow rate, which is measured by one of the two rotameters. Power input to the immersion heater inside the deaeration chamber is readjusted to achieve the desired liquid temperature. Additional liquid temperature control is achieved with the aid of the in-line electrical heater and the air-cooled heat exchanger. For experiments demanding high liquid temperatures, heat loss downstream of the deaeration chamber is compensated for by the in-line heater. On the other hand, low temperature (*i.e.*, high subcooling) experiments require significant cooling with

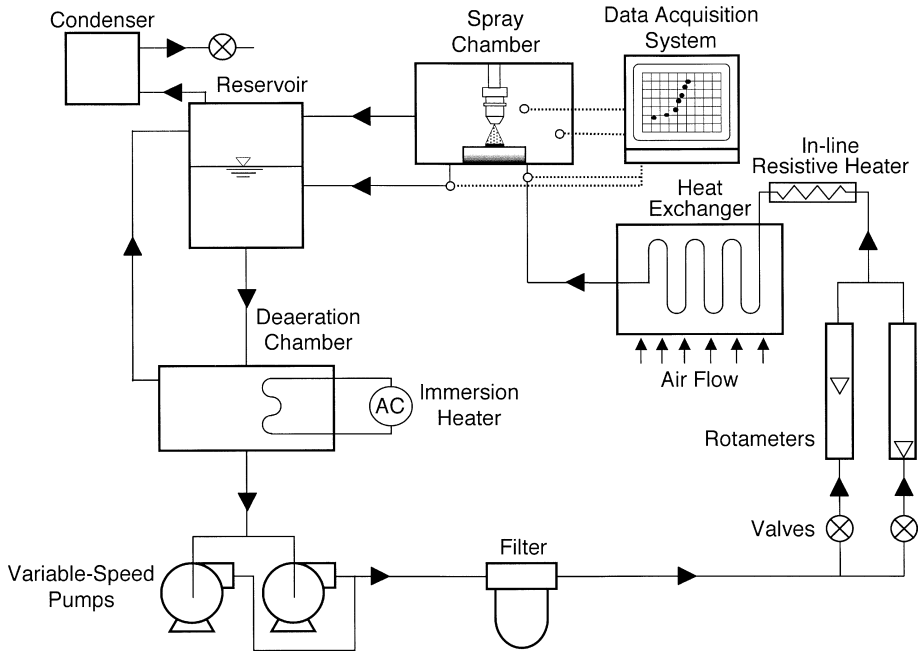

Fig. 1. Two-phase flow loop.

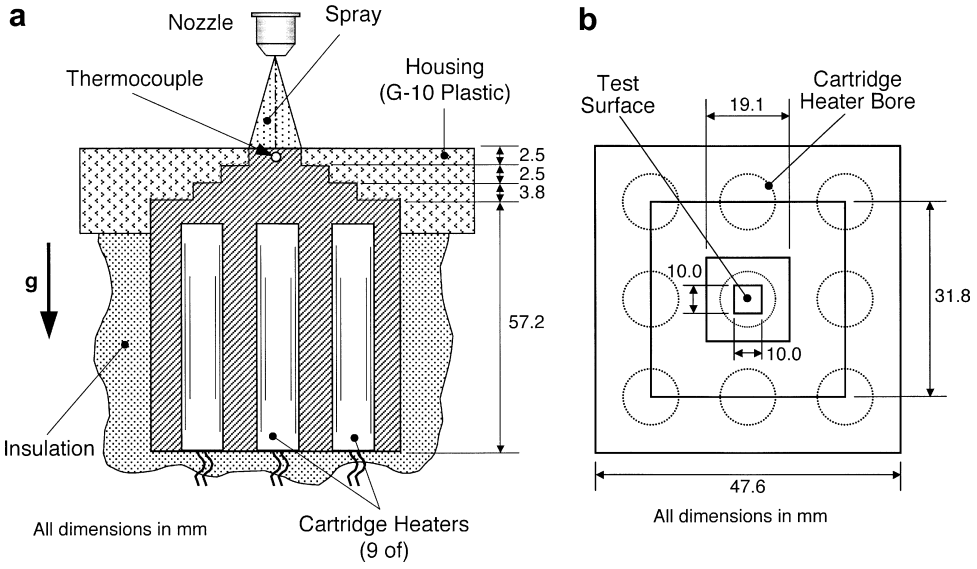

Fig. 2. (a) Sectional view of heater assembly. (b) Top view of copper block.

the aid of the air-cooled heat exchanger. Pressure inside the chamber is maintained at atmospheric level at all times.

Spray inlet liquid temperature and pressure are measured by sensors placed in the tubing leading to the nozzle, while sensors in the tubing exiting the spray chamber measure outlet temperature and pressure. Uncertainties in the pressure, flow rate and temperature measurements are estimated at less than 0.5%, 1.0% and ±0.2 °C, respectively.

A variable voltage transformer is used to supply power to the cartridge heaters embedded in the heater block. Power input is measured by a Yokogawa digital wattmeter having a measurement accuracy of 0.5%. Thermal analysis of the test heater shows only 2% of the electrical power input is lost to the ambient. This value was obtained from a three-dimensional model of the test module, including the copper block, G-10 plastic housing, and insulation, and accounting for external natural convection. Heat flux from the test surface is therefore determined by dividing the measured electrical power input by the 1×1 cm^2 test surface area.

Boiling curves are generated by increasing electrical power input to the heater in small increments and waiting until the heater temperature reaches steady state before recording power input and temperature data. Small power increments ensure accurate CHF measurement. CHF is detected by an unsteady and continuous rise in the heater temperature, at which point power input is quickly turned off.

3. Experimental results

Three Unijet full-cone pressure spray nozzles made by Spraying Systems Company were tested. These are the same nozzles used in previous FC-72 and PF 5052 studies [6,7,10–12]. Table 1 lists key hydrodynamic properties of these nozzles.

Table 1
Characteristics of spray nozzles used in present study

Nozzle	Orifice diameter d_0 (mm)	Spray angle θ (°)	Sauter mean diameter $d_{32} \times 10^6$ (m)	Volumetric flow rate $Q \times 10^6$ ($m^3\ s^{-1}$)
1	0.762	55.8	111–123	3.50–3.86
2	1.19	46.4	160–179	4.97–13.4
3	1.70	48.5	189–249	7.78–101

To ensure consistency in the present data as well as in comparing present and previous data, all present tests conformed to the orifice-to-surface distance criterion developed by Estes and Mudawar [7]. This criterion is based on the observation that CHF for a square test surface is highest when orifice-to-surface distance is adjusted such that the spray impact area just inscribe the square surface, *i.e.*, when the diameter of the impact area equal test heater width.

Experiments were performed using FC-77 as coolant, covering a flow rate range of $Q = 3.33 \times 10^{-6}$–20.4×10^{-6} m^3/s and subcoolings of ΔT_{sub} = 20.6–72 °C. Fig. 3a–c shows the effects of flow rate on boiling curves for nozzles 1–3 (see Table 1 for nozzle designation), respectively, at 72 °C subcooling. These figures show increasing the flow rate increases the single-phase heat transfer coefficient and delays the onset of boiling. However, the effect of flow rate is relatively insignificant in the nucleate boiling region. For each nozzle, CHF increases with increasing flow rate. Interestingly, CHF for nozzle 1 at a flow rate of 4.03×10^{-6} m^3/s is 220 W/cm^2 compared to only 190 W/cm^2 for nozzle 2 at a higher flow rate of 5.07×10^{-6} m^3/s. This seemingly inconsistent trend can be explained by the smaller droplet diameter for nozzle 1 ($d_{32} = 1.10 \times 10^{-4}$ m) compared to nozzle 2 ($d_{32} = 2.07 \times 10^{-4}$ m). Similar observations can be made when comparing data for nozzle 2 and nozzle 3. This shows CHF increases with increasing flow rate and/or decreasing droplet diameter.

Fig. 4a–c shows the effects of subcooling for a fixed flow rate for nozzles 1–3, respectively. These figures show increasing subcooling delays the onset of boiling and decreases the slope of the nucleate boiling region. For each nozzle, CHF increases monotonically with increasing subcooling; the increase is mild at low subcooling but becomes more pronounced at high subcooling. For nozzle 3, with a flow rate of 20.4×10^{-6} m^3/s, increasing the subcooling from 22 to 70 °C increases CHF from 158 to 320 W/cm^2, about a 100% enhancement. This proves high subcooling is a very effective means for removing high-heat fluxes in spray cooling.

4. Compilation of CHF database

To accomplish the goal of developing a CHF correlation that is valid for different spray nozzles, fluids, flow rates, droplet diameters, and orientations in additional to a broad range of subcooling, the present FC-77 data are combined with several prior databases. The complete database, which is detailed in Table 2, consists of two main parts. The first part is comprised of dielectric fluid data and the second part water data. As indicated in Table 3, the thermophysical properties of water are drastically different from those for dielectric fluids. Such large property differences are crucial to the development of a universal CHF correlation.

The first part of the database, which includes the present FC-77 data, consists of dielectric fluid data that conform to the aforementioned criterion of impact area that just inscribe the square test surface. This criterion is met by setting the orifice-to-surface distance such that the diameter of the spray impact area equal the width of the test surface. Using FC-72 as working fluid and downward oriented sprays, Mudawar and Estes experimentally demonstrated the merits of this criterion [7]. They showed that a very small orifice-to-surface distance causes only a small portion of the test surface area to be directly impacted by the spray droplets. On the other hand, a very large orifice-to-surface distance produces a very large impact area that extends well beyond the outer edges of the test surface, causing much of the coolant to be wasted. Both conditions were observed to yield low CHF values. The high-

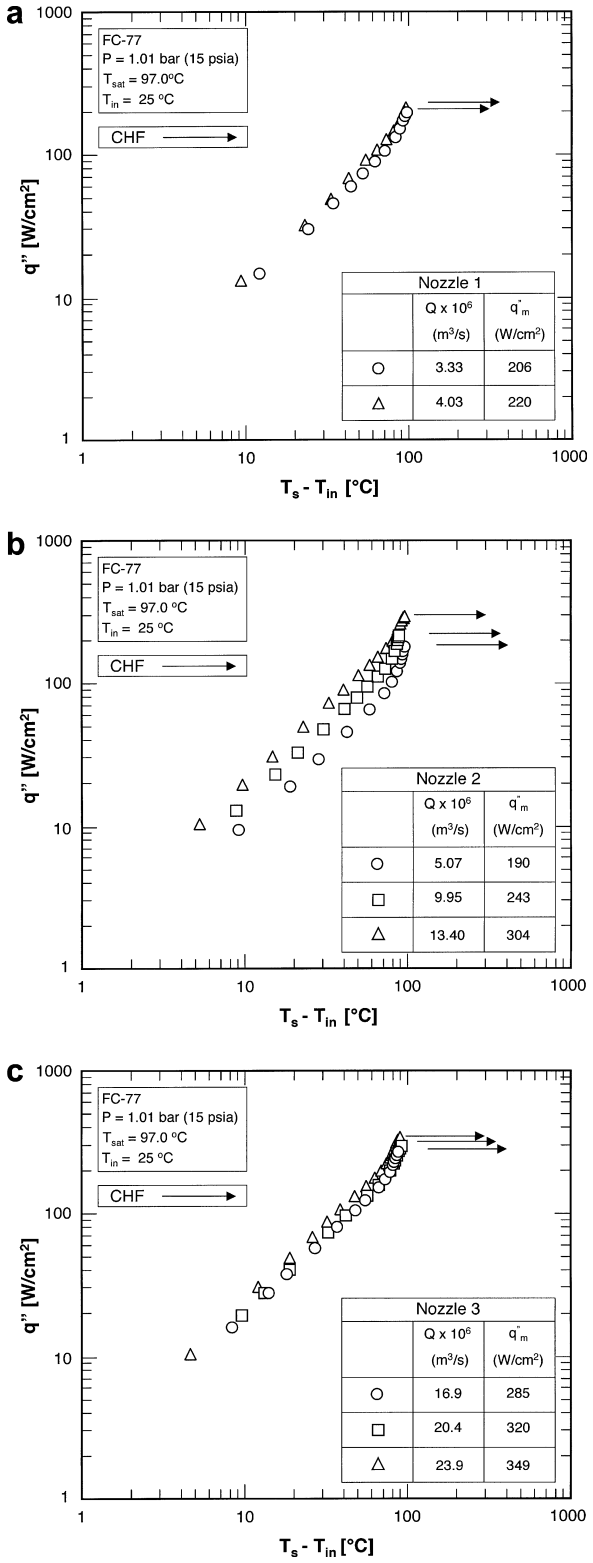

Fig. 3. Boiling curves for different flow rates at 72 °C subcooling for (a) nozzle 1, (b) nozzle 2, and (c) nozzle 3.

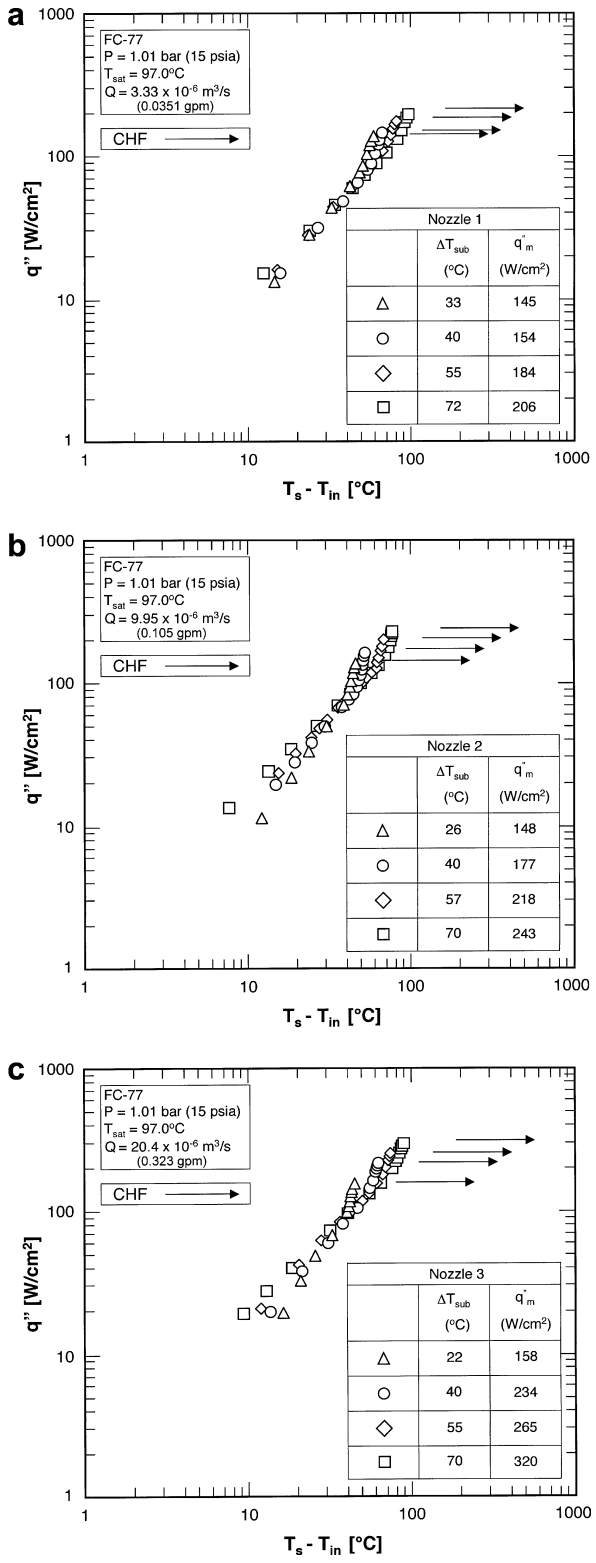

Fig. 4. Boiling curves for different subcoolings for (a) nozzle 1 at $Q = 3.33 \times 10^{-6}$ m^3/s, (b) nozzle 2 at $Q = 9.95 \times 10^{-6}$ m^3/s, and (c) nozzle 3 at $Q = 2.04 \times 10^{-5}$ m^3/s.

est CHF was achieved when the orifice-to-surface distance was adjusted such that the impact diameter just equals the width of the test surface. This criterion was therefore adopted in all studies upon which this portion of the database is based. Another important variable in the database is spray orientation as illustrated in Fig. 5. Using PF-5052 as working fluid, Rybicki and Mudawar [10] showed upward-oriented sprays produce cooling performance identical to that of downward-facing sprays. Also using PF-5052, the authors of the present study investigated the influence of spray inclination [11,12]. Sprays were tested at orientations ranging from normal to 60° from normal, with the major axis of the inclined spray equal to the width of the test surface. Increasing the spray inclination angle away from normal produced a fairly monotonic decrease in CHF. In summary, the first portion of the CHF database consists of data for following cases:

1. Normal downward-facing FC-72 sprays, Fig. 5a, by Estes and Mudawar [6,7].
2. Present normal downward-facing FC-77 sprays, Fig. 5a.
3. Normal upward-facing PF-5052 sprays, Fig. 5b, by Rybicki and Mudawar [10].
4. Inclined downward-facing PF-5052 sprays, Fig. 5c, by Visaria and Mudawar [11,12].

The same three full-cone spray nozzles (1–3) were used in all the above studies.

The second part of the CHF database consists of water data by Mudawar and Valentine [3]. Data are available for three full-cone spray nozzles (4–6) whose characteristics are detailed in Table 4. These data were obtained with downward-facing sprays. However, unlike the dielectric fluid data of the first part of the database, the orifice-to-surface distance for the water sprays was such that the spray impact area greatly exceeded the test surface area as illustrated in Fig. 5d.

4.1. Subcooling influence

Fig. 6 shows the variation of CHF with subcooling for nozzles 1–3 for different fluids, flow rates and subcoolings. For each nozzle, fairly similar values of flow rate are selected for the three dielectric fluids. Fig. 6 shows CHF increases fairly linearly with subcooling for each nozzle. Excepting nozzle 1 FC-72 data and nozzle 3 PF-5052 data, slopes appear fairly similar and point to a generalized trend of CHF with subcooling. Departure of these two data sets might be the result of the limited number of data points (three in each case) precluding accurate determination of the slope for these cases. Overall, there is some departure in CHF magnitude among the three fluids because of differences in thermophysical properties, with PF-5052 producing the highest CHF for a given level of subcooling, followed by FC-77 and FC-72. This can be explained by PF-5052 having the highest surface tension among the three fluids, thereby producing the smallest droplets.

4.2. Subcooled CHF correlation

Mudawar and Valentine [3] recommended a generalized CHF dimensionless correlation form for water sprays. Characteristic velocity and characteristic length were based on local volumetric flux, Q'', and Sauter mean diameter, d_{32}, respectively. The test surface they used was circular and much smaller than the impact area of the spray. Therefore, the local volumetric flux measured at the center of their sprays was equal to the mean volumetric flux impacting their test surface, $Q'' = \overline{Q}''$.

The correlation form proposed by Mudawar and Valentine was later modified by Estes and Mudawar [6,7] to correlate their FC-72 data. One key difference between the two studies was size of the test surface. For the FC-72 data, the spray impact area just inscribed the test heater. This caused appreciable variation of volumetric flux across the impact area. Using a point-source volumetric flux model [7], the magnitude of local volumetric flux, Q'', along the outer edge of the impact area was related to the average volumetric flux, $\overline{Q}''$, by the relation

Table 2
Spray CHF database

No.	Fluid	θ (°)	T_{in} (°C)	T_s (°C)	T_{sat} (°C)	ΔT_{sub} (°C)	Q (m^3/s)	ΔP (N/m^2)	CHF (W/cm^2)	Q'' (m/s)	$\overline{Q}''$ (m/s)	d_{32} (m)	*We*
1	PF-5052	55.8	25.9	82.7	50.0	24.1	3.86×10^{-6}	1.52×10^{5}	146.0	0.0409	0.0492	9.83×10^{-5}	0.0224
2	PF-5052	55.8	25.4	84.9	50.0	24.6	3.86×10^{-6}	1.29×10^{5}	175.0	0.0409	0.0492	1.02×10^{-4}	0.0232
3	PF-5052	46.4	35.2	84.1	50.0	14.8	9.91×10^{-6}	7.81×10^{4}	160.0	0.1112	0.1261	1.50×10^{-4}	0.2506
4	PF-5052	46.4	35.2	85.9	50.0	14.8	1.35×10^{-5}	1.43×10^{5}	175.0	0.1512	0.1714	1.28×10^{-4}	0.3944
5	PF-5052	46.4	35.1	80.2	50.0	14.9	4.93×10^{-6}	2.74×10^{4}	113.0	0.0553	0.0627	1.99×10^{-4}	0.0822
6	PF-5052	46.4	26.4	86.2	50.0	23.6	1.35×10^{-5}	1.44×10^{5}	192.0	0.1512	0.1714	1.30×10^{-4}	0.4023
7	PF-5052	46.4	26.1	85.8	50.0	23.9	9.91×10^{-6}	7.97×10^{4}	180.0	0.1112	0.1261	1.52×10^{-4}	0.2542
8	PF-5052	46.4	25.2	83.2	50.0	24.8	4.93×10^{-6}	2.77×10^{4}	148.0	0.0553	0.0627	2.00×10^{-4}	0.0834
9	PF-5052	48.5	35.1	84.7	50.0	14.9	1.70×10^{-5}	7.66×10^{4}	172.0	0.1889	0.2167	1.88×10^{-4}	0.9029
10	PF-5052	48.5	26.4	87.9	50.0	23.6	1.70×10^{-5}	7.87×10^{4}	202.0	0.1889	0.3167	1.88×10^{-4}	0.9095
11	PF-5052[a]	55.8	27.0	73.2	50.0	23.0	1.29×10^{-6}	9.93×10^{4}	138.0	0.0328	0.0394	1.11×10^{-4}	0.0164
12	PF-5052[a]	55.8	27.0	74.7	50.0	23.0	1.53×10^{-6}	1.15×10^{5}	147.2	0.0365	0.0438	1.07×10^{-4}	0.0194
13	PF-5052[a]	55.8	27.0	73.8	50.0	23.0	1.78×10^{-6}	1.36×10^{5}	152.1	0.0402	0.0483	1.02×10^{-4}	0.0226
14	PF-5052[a]	55.8	24.8	75.3	50.0	25.2	1.52×10^{-6}	1.20×10^{5}	158.7	0.0365	0.0438	1.06×10^{-4}	0.0193
15	PF-5052[a]	55.8	23.7	74.6	50.0	26.3	1.31×10^{-6}	9.38×10^{4}	146.9	0.0328	0.0394	1.13×10^{-4}	0.0167
16	PF-5052[a]	55.8	23.1	74.8	50.0	26.9	1.79×10^{-6}	1.36×10^{5}	161.2	0.0402	0.0483	1.03×10^{-4}	0.0228
17	PF-5052[a]	46.4	37.7	69.9	50.0	12.3	3.04×10^{-5}	9.49×10^{4}	125.3	0.1252	0.1420	1.82×10^{-4}	0.3874
18	PF-5052[a]	46.4	36.5	69.9	50.0	13.5	1.80×10^{-5}	6.11×10^{4}	125.0	0.1013	0.1149	1.64×10^{-4}	0.2296
19	PF-5052[a]	46.4	35.3	71.6	50.0	14.7	2.09×10^{-5}	7.57×10^{4}	134.9	0.1122	0.1272	1.55×10^{-4}	0.2661
20	PF-5052[a]	46.4	27.0	72.1	50.0	23.0	1.83×10^{-5}	6.24×10^{4}	166.0	0.1013	0.1149	1.65×10^{-4}	0.2625
21	PF-5052[a]	46.4	27.0	72.0	50.0	23.0	2.12×10^{-5}	7.69×10^{4}	173.5	0.1122	0.1272	1.57×10^{-4}	0.2703
22	PF-5052[a]	46.4	27.0	72.2	50.0	23.0	2.49×10^{-5}	9.55×10^{4}	189.8	0.1249	0.1416	1.48×10^{-4}	0.3165
23	PF-5052[a]	46.4	24.4	74.6	50.0	25.6	2.47×10^{-5}	9.87×10^{4}	200.0	0.1249	0.1416	1.47×10^{-4}	0.3139
24	PF-5052[a]	46.4	24.1	71.4	50.0	25.9	1.83×10^{-5}	6.37×10^{4}	177.1	0.1013	0.1149	1.65×10^{-4}	0.2333
25	PF-5052[a]	46.4	23.9	72.6	50.0	26.1	2.12×10^{-5}	7.94×10^{4}	179.1	0.1122	0.1272	1.56×10^{-4}	0.2696
26	PF-5052[a]	48.5	38.0	72.3	50.0	12.0	6.90×10^{-5}	7.33×10^{4}	136.5	0.1829	0.2099	1.93×10^{-4}	0.8779
27	PF-5052[a]	48.5	38.0	71.6	50.0	12.0	9.54×10^{-5}	1.33×10^{5}	145.2	0.2323	0.2665	1.66×10^{-4}	1.2151
28	PF-5052[a]	48.5	37.0	70.4	50.0	13.0	4.50×10^{-5}	4.06×10^{4}	117.0	0.1364	0.1565	2.26×10^{-4}	0.5732
29	PF-5052[a]	48.5	27.5	70.2	50.0	22.5	4.60×10^{-5}	4.09×10^{4}	166.1	0.1364	0.1565	2.30×10^{-4}	0.5862
30	PF-5052[a]	48.5	27.0	71.7	50.0	23.0	7.07×10^{-5}	7.46×10^{4}	196.0	0.1829	0.2099	1.96×10^{-4}	0.8997
31	PF-5052[a]	48.5	26.7	73.8	50.0	23.3	1.00×10^{-4}	1.19×10^{5}	227.6	0.2323	0.2665	1.73×10^{-4}	1.2796
32	PF-5052[a]	48.5	24.0	72.1	50.0	26.0	4.60×10^{-5}	4.17×10^{4}	185.4	0.1364	0.1565	2.29×10^{-4}	0.5854
33	PF-5052[a]	48.5	24.0	72.4	50.0	26.0	1.01×10^{-4}	1.21×10^{5}	236.7	0.2323	0.2665	1.74×10^{-4}	1.2864
34	PF-5052[a]	48.5	22.4	70.9	50.0	27.6	7.15×10^{-5}	7.51×10^{4}	212.9	0.1829	0.2099	1.98×10^{-4}	0.9101
35	FC-72	55.8	43.0	–	56.0	13.0	1.57×10^{-6}	6.82×10^{4}	74.0	0.0166	0.0200	3.65×10^{-4}	0.0135
36	FC-72	55.8	43.0	–	56.0	13.0	1.88×10^{-6}	8.18×10^{4}	68.0	0.0200	0.0240	3.55×10^{-4}	0.0189
37	FC-72	55.8	43.0	–	56.0	13.0	2.20×10^{-6}	9.54×10^{4}	75.0	0.0233	0.0280	3.44×10^{-4}	0.0249
38	FC-72	55.8	43.0	–	56.0	13.0	2.51×10^{-6}	1.09×10^{5}	83.0	0.0266	0.0320	3.32×10^{-4}	0.0314
39	FC-72	55.8	43.0	–	56.0	13.0	2.83×10^{-6}	1.23×10^{5}	88.0	0.0300	0.0360	3.20×10^{-4}	0.0383
40	FC-72	55.8	43.0	–	56.0	13.0	3.14×10^{-6}	1.36×10^{5}	92.0	0.0333	0.0400	3.08×10^{-4}	0.0456
41	FC-72	55.8	43.0	–	56.0	13.0	3.46×10^{-6}	1.50×10^{5}	98.0	0.0366	0.0440	2.98×10^{-4}	0.0534
42	FC-72	55.8	43.0	–	56.0	13.0	3.77×10^{-6}	1.64×10^{5}	120.0	0.0400	0.0480	2.89×10^{-4}	0.0616
43	FC-72	55.8	43.0	–	56.0	13.0	4.08×10^{-6}	1.77×10^{5}	126.0	0.0433	0.0520	2.81×10^{-4}	0.0703
44	FC-72	55.8	43.0	–	56.0	13.0	4.40×10^{-6}	1.91×10^{5}	132.0	0.0466	0.0560	2.74×10^{-4}	0.0794
45	FC-72	55.8	43.0	–	56.0	13.0	4.71×10^{-6}	2.04×10^{5}	136.0	0.0499	0.0600	2.67×10^{-4}	0.0889
46	FC-72	55.8	43.0	–	56.0	13.0	4.95×10^{-6}	2.15×10^{5}	138.0	0.0524	0.0630	2.61×10^{-4}	0.0958
47	FC-72	55.8	33.0	–	56.0	23.0	1.57×10^{-5}	6.82×10^{5}	74.0	0.0166	0.0200	3.83×10^{-4}	0.0135
48	FC-72	55.8	33.0	–	56.0	23.0	1.88×10^{-5}	8.18×10^{4}	76.0	0.0200	0.0240	3.73×10^{-4}	0.0189
49	FC-72	55.8	33.0	–	56.0	23.0	2.20×10^{-5}	9.54×10^{4}	80.0	0.0266	0.0280	3.61×10^{-4}	0.0249
50	FC-72	55.8	33.0	–	56.0	23.0	2.51×10^{-6}	1.09×10^{5}	88.0	0.0266	0.0320	3.48×10^{-4}	0.0314
51	FC-72	55.8	33.0	–	56.0	23.0	2.83×10^{-6}	1.23×10^{5}	94.0	0.0300	0.0360	3.36×10^{-4}	0.0383
52	FC-72	55.8	33.0	–	56.0	23.0	3.14×10^{-6}	1.36×10^{5}	106.0	0.0333	0.0400	3.24×10^{-4}	0.0456
53	FC-72	55.8	33.0	–	56.0	23.0	3.46×10^{-6}	1.50×10^{5}	108.0	0.0366	0.0440	3.13×10^{-4}	0.0534
54	FC-72	55.8	33.0	–	56.0	23.0	3.77×10^{-6}	1.64×10^{5}	116.0	0.0400	0.0480	3.04×10^{-4}	0.0616
55	FC-72	55.8	33.0	–	56.0	23.0	4.08×10^{-6}	1.77×10^{5}	119.0	0.0433	0.0520	2.95×10^{-4}	0.0703
56	FC-72	55.8	33.0	–	56.0	23.0	4.40×10^{-6}	1.91×10^{5}	122.0	0.0466	0.0560	2.87×10^{-4}	0.0794
57	FC-72	55.8	33.0	–	56.0	23.0	4.71×10^{-6}	2.04×10^{5}	127.0	0.0499	0.0600	2.80×10^{-4}	0.0889
58	FC-72	55.8	33.0	–	56.0	23.0	4.95×10^{-6}	2.15×10^{5}	130.0	0.0524	0.0630	2.74×10^{-4}	0.0958
59	FC-72	55.8	23.0	–	56.0	33.0	1.57×10^{-6}	6.82×10^{4}	80.0	0.0166	0.0200	4.01×10^{-4}	0.0135
60	FC-72	55.8	23.0	–	56.0	33.0	1.88×10^{-6}	8.18×10^{4}	82.0	0.0200	0.0240	3.90×10^{-4}	0.0189
61	FC-72	55.8	23.0	–	56.0	33.0	2.20×10^{-6}	9.54×10^{4}	90.0	0.0233	0.0280	3.77×10^{-4}	0.0249
62	FC-72	55.8	23.0	–	56.0	33.0	2.51×10^{-6}	1.09×10^{5}	100.0	0.0266	0.0320	3.64×10^{-4}	0.0314
63	FC-72	55.8	23.0	–	56.0	33.0	2.83×10^{-6}	1.23×10^{5}	106.0	0.0300	0.0360	3.51×10^{-4}	0.0383
64	FC-72	55.8	23.0	–	56.0	33.0	3.14×10^{-6}	1.36×10^{5}	111.0	0.0333	0.0400	3.39×10^{-4}	0.0456
65	FC-72	55.8	23.0	–	56.0	33.0	3.46×10^{-6}	1.50×10^{5}	117.0	0.0366	0.0440	3.28×10^{-4}	0.0534
66	FC-72	55.8	23.0	–	56.0	33.0	3.77×10^{-6}	1.64×10^{5}	129.0	0.0400	0.0480	3.18×10^{-4}	0.0616
67	FC-72	55.8	23.0	–	56.0	33.0	4.08×10^{-6}	1.77×10^{5}	140.0	0.0433	0.0520	3.09×10^{-4}	0.0703
68	FC-72	55.8	23.0	–	56.0	33.0	4.40×10^{-6}	1.91×10^{5}	150.0	0.0466	0.0560	3.01×10^{-4}	0.0794
69	FC-72	55.8	23.0	–	56.0	33.0	4.71×10^{-6}	2.04×10^{5}	154.0	0.0499	0.0600	2.93×10^{-4}	0.0889
70	FC-72	55.8	23.0	–	56.0	33.0	4.95×10^{-6}	2.15×10^{5}	158.0	0.0524	0.0630	2.87×10^{-4}	0.0958
71	FC-72	46.4	43.0	–	56.0	13.0	4.95×10^{-6}	2.15×10^{5}	72.0	0.0556	0.0630	3.73×10^{-4}	0.1535
72	FC-72	46.4	43.0	–	56.0	13.0	5.58×10^{-6}	2.42×10^{5}	78.0	0.0626	0.0710	3.68×10^{-4}	0.1925
73	FC-72	46.4	43.0	–	56.0	13.0	7.54×10^{-6}	3.27×10^{5}	86.0	0.0847	0.0960	3.47×10^{-4}	0.3316
74	FC-72	46.4	43.0	–	56.0	13.0	8.56×10^{-6}	3.72×10^{5}	92.0	0.0961	0.1090	3.35×10^{-4}	0.4130
75	FC-72	46.4	43.0	–	56.0	13.0	9.66×10^{-6}	4.19×10^{5}	96.0	0.1085	0.1230	3.24×10^{-4}	0.5094
76	FC-72	46.4	43.0	–	56.0	13.0	1.07×10^{-5}	4.64×10^{5}	98.0	0.1199	0.1360	3.15×10^{-4}	0.6043
77	FC-72	46.4	43.0	–	56.0	13.0	1.18×10^{-5}	5.11×10^{5}	98.0	0.1323	0.1500	3.07×10^{-4}	0.7160

Table 2 (*continued*)

No.	Fluid	θ (°)	T_{in} (°C)	T_s (°C)	T_{sat} (°C)	ΔT_{sub} (°C)	Q (m^3/s)	ΔP (N/m^2)	CHF (W/cm^2)	Q'' (m/s)	$\overline{Q}''$ (m/s)	d_{32} (m)	*We*
78	FC-72	46.4	33.0	–	56.0	23.0	4.95×10^{-6}	2.15×10^{5}	91.0	0.0556	0.0630	3.91×10^{-4}	0.1535
79	FC-72	46.4	33.0	–	56.0	23.0	5.58×10^{-6}	2.42×10^{5}	96.0	0.0626	0.0710	3.86×10^{-4}	0.1925
80	FC-72	46.4	33.0	–	56.0	23.0	7.54×10^{-6}	3.27×10^{5}	112.0	0.0847	0.0960	3.64×10^{-4}	0.3316
81	FC-72	46.4	33.0	–	56.0	23.0	8.56×10^{-6}	3.72×10^{5}	120.0	0.0961	0.1090	3.52×10^{-4}	0.4130
82	FC-72	46.4	33.0	–	56.0	23.0	9.66×10^{-6}	4.19×10^{5}	131.0	0.1085	0.1230	3.41×10^{-4}	0.5094
83	FC-72	46.4	33.0	–	56.0	23.0	1.07×10^{-5}	4.64×10^{5}	136.0	0.1199	0.1360	3.30×10^{-4}	0.6043
84	FC-72	46.4	33.0	–	56.0	23.0	1.18×10^{-5}	5.11×10^{5}	142.0	0.1323	0.1500	3.22×10^{-4}	0.7161
85	FC-72	46.4	33.0	–	56.0	23.0	1.29×10^{-5}	5.59×10^{5}	146.0	0.1446	0.1640	3.14×10^{-4}	0.8353
86	FC-72	46.4	33.0	–	56.0	23.0	1.29×10^{-5}	5.59×10^{5}	98.0	0.1446	0.1640	3.14×10^{-4}	0.8353
87	FC-72	46.4	23.0	–	56.0	33.0	4.95×10^{-6}	2.15×10^{5}	98.0	0.0556	0.0630	4.09×10^{-4}	0.1535
88	FC-72	46.4	23.0	–	56.0	33.0	5.58×10^{-6}	2.42×10^{5}	105.0	0.0626	0.0710	4.04×10^{-4}	0.1925
89	FC-72	46.4	23.0	–	56.0	33.0	7.54×10^{-6}	3.27×10^{5}	124.0	0.0847	0.0960	3.81×10^{-4}	0.3316
90	FC-72	46.4	23.0	–	56.0	33.0	8.56×10^{-6}	3.72×10^{5}	136.0	0.0961	0.1090	3.68×10^{-4}	0.4130
91	FC-72	46.4	23.0	–	56.0	33.0	9.66×10^{-6}	4.19×10^{5}	148.0	0.1085	0.1230	3.56×10^{-4}	0.5094
92	FC-72	46.4	23.0	–	56.0	33.0	1.07×10^{-5}	4.64×10^{5}	164.0	0.1199	0.1360	3.46×10^{-4}	0.6043
93	FC-72	46.4	23.0	–	56.0	33.0	1.18×10^{-5}	5.11×10^{5}	173.0	0.1323	0.1500	3.37×10^{-4}	0.7161
94	FC-72	46.4	23.0	–	56.0	33.0	1.29×10^{-5}	5.59×10^{5}	182.0	0.1446	0.1640	3.29×10^{-4}	0.8353
95	FC-72	48.5	43.0	–	56.0	13.0	7.78×10^{-6}	3.37×10^{5}	80.0	0.0863	0.0990	3.63×10^{-4}	0.3607
96	FC-72	48.5	43.0	–	56.0	13.0	9.74×10^{-6}	4.23×10^{5}	90.0	0.1081	0.1240	3.60×10^{-4}	0.5609
97	FC-72	48.5	43.0	–	56.0	13.0	1.17×10^{-5}	5.08×10^{5}	101.0	0.1299	0.1490	3.50×10^{-4}	0.7876
98	FC-72	48.5	43.0	–	56.0	13.0	1.37×10^{-5}	5.93×10^{5}	108.0	0.1516	0.1740	3.38×10^{-4}	1.0382
99	FC-72	48.5	43.0	–	56.0	13.0	1.56×10^{-5}	6.75×10^{5}	114.0	0.1726	0.1980	3.27×10^{-4}	1.3006
100	FC-72	48.5	43.0	–	56.0	13.0	1.75×10^{-5}	7.60×10^{5}	122.0	0.1944	0.2230	3.18×10^{-4}	1.6009
101	FC-72	48.5	43.0	–	56.0	13.0	1.95×10^{-5}	8.45×10^{5}	127.0	0.2161	0.2480	3.09×10^{-4}	1.9276
102	FC-72	48.5	33.0	–	56.0	23.0	7.78×10^{-6}	3.37×10^{5}	86.0	0.0863	0.0990	3.81×10^{-4}	0.3607
103	FC-72	48.5	33.0	–	56.0	23.0	9.74×10^{-6}	4.23×10^{5}	108.0	0.1081	0.1240	3.78×10^{-4}	0.5609
104	FC-72	48.5	33.0	–	56.0	23.0	1.17×10^{-5}	5.08×10^{5}	122.0	0.1299	0.1490	3.67×10^{-4}	0.7876
105	FC-72	48.5	33.0	–	56.0	23.0	1.37×10^{-5}	5.93×10^{5}	130.0	0.1516	0.1740	3.55×10^{-4}	1.0382
106	FC-72	48.5	33.0	–	56.0	23.0	1.56×10^{-5}	6.75×10^{5}	143.0	0.1726	0.1980	3.44×10^{-4}	1.3006
107	FC-72	48.5	33.0	–	56.0	23.0	1.75×10^{-5}	7.60×10^{5}	148.0	0.1944	0.2230	3.33×10^{-4}	1.6009
108	FC-72	48.5	33.0	–	56.0	23.0	1.95×10^{-5}	8.45×10^{5}	153.0	0.2161	0.2480	3.25×10^{-4}	1.9276
109	FC-72	48.5	23.0	–	56.0	33.0	7.78×10^{-6}	3.37×10^{5}	122.0	0.0863	0.0990	3.99×10^{-4}	0.3607
110	FC-72	48.5	23.0	–	56.0	33.0	9.74×10^{-6}	4.23×10^{5}	138.0	0.1081	0.1240	3.95×10^{-4}	0.5609
111	FC-72	48.5	23.0	–	56.0	33.0	1.17×10^{-5}	5.08×10^{5}	155.0	0.1299	0.1490	3.84×10^{-4}	0.7876
112	FC-72	48.5	23.0	–	56.0	33.0	1.37×10^{-5}	5.93×10^{5}	160.0	0.1516	0.1740	3.72×10^{-4}	1.0382
113	FC-72	48.5	23.0	–	56.0	33.0	1.56×10^{-5}	6.75×10^{5}	168.0	0.1726	0.1980	3.59×10^{-4}	1.3006
114	FC-72	48.5	23.0	–	56.0	33.0	1.75×10^{-5}	7.60×10^{5}	186.0	0.1944	0.2230	3.49×10^{-4}	1.6009
115	FC-72	48.5	23.0	–	56.0	33.0	1.95×10^{-5}	8.45×10^{5}	199.0	0.2161	0.2480	3.40×10^{-4}	1.9276
116	FC-77	55.8	64.2	128.3	97.0	32.8	3.33×10^{-6}	1.10×10^{5}	145.0	0.0353	0.0424	1.03×10^{-4}	0.0248
117	FC-77	55.8	57.0	126.6	97.0	40.0	3.33×10^{-6}	1.12×10^{5}	154.0	0.0353	0.0424	1.05×10^{-4}	0.0245
118	FC-77	55.8	42.3	128.9	97.0	54.7	3.33×10^{-6}	1.18×10^{5}	184.0	0.0353	0.0424	1.09×10^{-4}	0.0243
119	FC-77	55.8	25.1	127.6	97.0	71.9	3.33×10^{-6}	1.11×10^{5}	203.0	0.0353	0.0424	1.18×10^{-4}	0.0247
120	FC-77	55.8	25.1	128.4	97.0	71.9	4.03×10^{-6}	1.53×10^{5}	220.0	0.0427	0.0513	1.10×10^{-4}	0.0338
121	FC-77	46.4	71.2	122.2	97.0	25.8	9.96×10^{-6}	8.81×10^{4}	148.0	0.1118	0.1268	1.43×10^{-4}	0.3467
122	FC-77	46.4	63.8	121.0	97.0	33.2	9.96×10^{-6}	8.98×10^{4}	177.0	0.1118	0.1268	1.47×10^{-4}	0.3449
123	FC-77	46.4	45.0	119.9	97.0	52.0	9.96×10^{-6}	9.20×10^{4}	218.0	0.1118	0.1268	1.57×10^{-4}	0.3433
124	FC-77	46.4	35.7	121.2	97.0	61.3	9.96×10^{-6}	9.41×10^{4}	243.0	0.1118	0.1268	1.62×10^{-4}	0.3450
125	FC-77	46.4	28.5	117.5	97.0	68.5	5.08×10^{-6}	4.11×10^{4}	190.0	0.0570	0.0645	2.07×10^{-4}	0.1107
126	FC-77	46.4	26.0	123.0	97.0	71.0	1.34×10^{-5}	1.57×10^{5}	304.0	0.1509	0.1711	1.50×10^{-4}	0.5675
127	FC-77	48.5	76.4	126.5	97.0	20.6	2.04×10^{-5}	1.36×10^{5}	158.0	0.2265	0.2599	1.54×10^{-4}	1.5919
128	FC-77	48.5	57.4	127.1	97.0	39.6	2.04×10^{-5}	1.25×10^{5}	234.0	0.2265	0.2599	1.72×10^{-4}	1.6546
129	FC-77	48.5	42.2	124.8	97.0	54.8	2.04×10^{-5}	1.30×10^{5}	265.0	0.2265	0.2599	1.82×10^{-4}	1.6451
130	FC-77	48.5	27.0	126.9	97.0	70.0	2.04×10^{-5}	1.28×10^{5}	320.0	0.2265	0.2599	1.98×10^{-4}	1.7141
131	FC-77	48.5	27.0	129.4	97.0	70.0	2.39×10^{-5}	1.74×10^{5}	349.0	0.2652	0.3043	1.83×10^{-4}	2.1894
132	FC-77	48.5	26.2	123.5	97.0	70.8	1.69×10^{-5}	9.28×10^{4}	285.0	0.1878	0.2155	2.16×10^{-4}	1.2685
133	FC-77	48.5	25.2	128.6	97.0	71.8	1.34×10^{-5}	6.38×10^{4}	262.0	0.1491	0.1711	2.37×10^{-4}	0.8888
134	Water	15.0	80.0	–	100.0	20.0	–	5.52×10^{5}	215.0	0.0011	0.0011	4.25×10^{-4}	7.97×10^{-6}
135	Water	15.0	70.0	–	100.0	30.0	–	5.52×10^{5}	230.0	0.0011	0.0011	4.35×10^{-4}	7.97×10^{-6}
136	Water	15.0	60.0	–	100.0	40.0	–	5.52×10^{5}	242.0	0.0011	0.0011	4.45×10^{-4}	7.97×10^{-6}
137	Water	15.0	50.0	–	100.0	50.0	–	5.52×10^{5}	250.0	0.0011	0.0011	4.55×10^{-4}	7.97×10^{-6}
138	Water	15.0	40.0	–	100.0	60.0	–	5.52×10^{5}	270.0	0.0011	0.0011	4.64×10^{-4}	7.68×10^{-6}
139	Water	15.0	30.0	–	100.0	70.0	–	5.52×10^{5}	277.0	0.0010	0.0010	4.74×10^{-3}	7.13×10^{-6}
140	Water	45.0	23.0	–	100.0	77.0	–	2.76×10^{5}	134.0	0.0006	0.0006	6.48×10^{-3}	3.20×10^{-5}
141	Water	45.0	23.0	–	100.0	77.0	–	1.38×10^{5}	187.0	0.0010	0.0010	1.04×10^{-3}	1.43×10^{-5}
142	Water	45.0	23.0	–	100.0	77.0	–	2.76×10^{5}	241.0	0.0010	0.0010	6.45×10^{-4}	9.57×10^{-6}
143	Water	15.0	23.0	–	100.0	77.0	–	5.52×10^{5}	273.0	0.0010	0.0010	4.81×10^{-4}	6.46×10^{-6}
144	Water	15.0	23.0	–	100.0	77.0	–	1.38×10^{5}	285.0	0.0011	0.0011	4.80×10^{-4}	7.26×10^{-6}
145	Water	30.0	23.0	–	100.0	77.0	–	1.17×10^{5}	287.0	0.0020	0.0020	9.01×10^{-4}	5.04×10^{-5}
146	Water	45.0	23.0	–	100.0	77.0	–	5.52×10^{5}	423.0	0.0020	0.0020	5.76×10^{-4}	3.16×10^{-5}
147	Water	30.0	23.0	–	100.0	77.0	–	1.38×10^{5}	584.0	0.0050	0.0050	1.38×10^{-3}	4.72×10^{-4}
148	Water	15.0	23.0	–	100.0	77.0	–	2.55×10^{5}	638.0	0.0050	0.0050	5.83×10^{-4}	1.99×10^{-4}

[a] Data for vertical upward-facing sprays. All other data shown are for vertical downward-facing sprays. Inclined spray data are not listed.

$$\frac{Q''}{\overline{Q}''} = \frac{1}{2}[1 + \cos(\theta/2)]\cos(\theta/2), \quad (1)$$

where $\overline{Q}'' = Q/(\pi L^2/4)$. Because this local volumetric flux constitutes a minimum in the spatial distribution of volumetric flux across the

Table 3
Thermophysical properties of different fluids at one atmosphere

Fluid	T_{sat} (°C)	ρ_f (kg/m^3)	ρ_g (kg/m^3)	$\sigma \times 10^3$ (N/m)	h_{fg} (kJ/kg)	$c_{p,f}$ (J/kg K)	$\mu_f \times 10^6$ (N s/m^2)
Water	100	957.9	0.569	58.9	2257	4217	279.0
FC-77	97	1600.0	12.66	8.23	78.75	1164	454.0
FC-72	56	1616.4	13.72	9.37	84.20	1098	440.6
PF-5052	50	1642.5	12.00	13.0	104.7	1092	517.2
Properties at 23 °C							
Water	23	998.0	0.019	72.8	2449	4181	959.0
FC-77	23	1782.0	–	13.93	–	1050	1329
FC-72	23	1684.0	3.95	12.2	93.65	1045	662.6
PF-5052	23	1715.1	–	13.0	–	1050	703.2

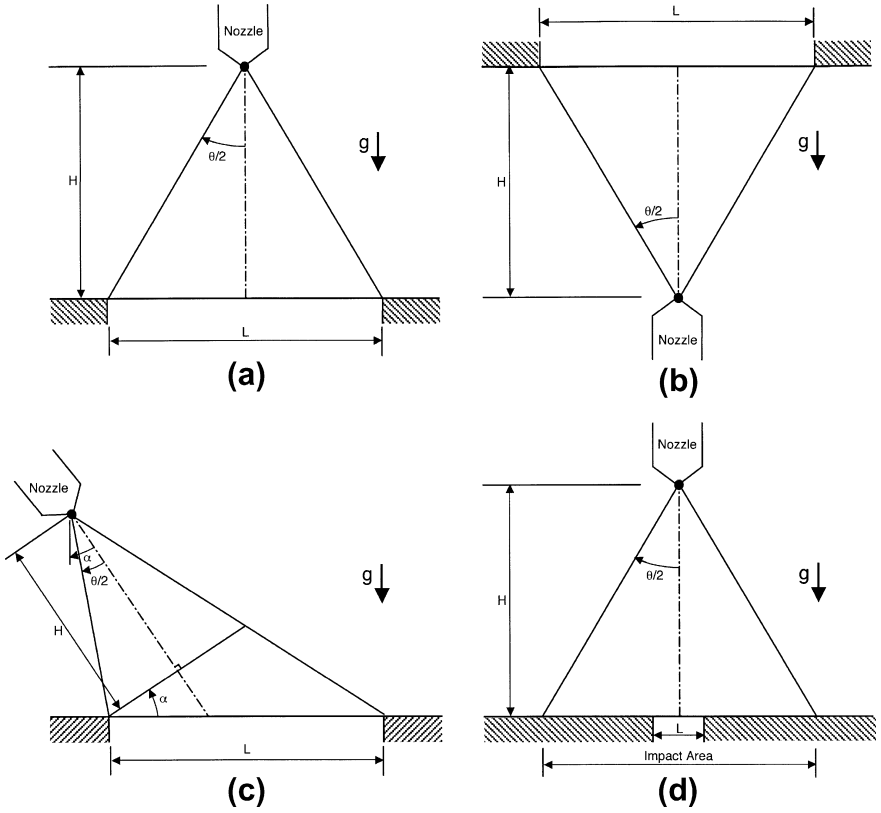

Fig. 5. Schematic representation of (a) downward-facing spray, (b) upward-facing spray, (c) inclined spray, and (d) downward-facing spray with small test surface.

Table 4
Characteristics of water spray nozzles used by Mudawar and Valentine [3]

Nozzle	Spray angle θ	Pressure difference $\Delta P \times 10^5$ (Pa)	Sauter mean diameter $d_{32} \times 10^6$ (m)	Volumetric flow rate $Q \times 10^6$ (m^3 s^{-1})
4	15	2.55–5.52	405–491	0.99–4.99
5	30	0.94–1.65	760–1258	2.02–9.96
6	45	0.69–5.52	485–1351	0.60–2.02

impact area, CHF is likely to occur along the outer edge of the impact area where the local (point-based) CHF, $q''_{m,p}$, is given by [6]

$$\frac{q''_{m,p}}{\rho_g h_{fg} Q''} = 2.3\left(\frac{\rho_f}{\rho_g}\right)^{0.3}\left(\frac{\rho_f Q''^2 d_{32}}{\sigma}\right)^{-0.35}\left(1+0.0019\frac{\rho_f c_{p,f}\Delta T_{sub}}{\rho_g h_{fg}}\right). \quad (2)$$

Sauter mean diameter, d_{32}, in Eq. (2) is given by [6]

$$\frac{d_{32}}{d_0} = 3.67[We_{d_0}^{1/2} Re_{d_0}]^{-0.259}, \quad (3)$$

where We_{d_0} and Re_{d_0} are Weber and Reynolds numbers based on orifice diameter and defined, respectively, as

$$We_{d_0} = \frac{\rho_g(2\Delta P/\rho_f)d_0}{\sigma} \quad (4)$$

and

$$Re_{d_0} = \frac{\rho_f(2\Delta P/\rho_f)^{1/2} d_0}{\mu_f}. \quad (5)$$

Notice that the measured CHF, q''_m, is based on the total area (L^2) of the test surface. Therefore, the local CHF along the outer edge of the spray impact area can be related to the measured CHF by the relation

$$q''_{m,p}(\pi L^2/4) = q''_m L^2. \quad (6)$$

The CHF correlation given by Eq. (2) was derived entirely from data for downward-facing FC-72 and water sprays. Rybicki and Mudawar [10] successfully used the same correlation for upward-facing PF-5052 sprays. Later, the authors of the present study validated this correlation for inclined PF-5052 sprays as well [11,12]. This demonstrates the effectiveness and universal validity

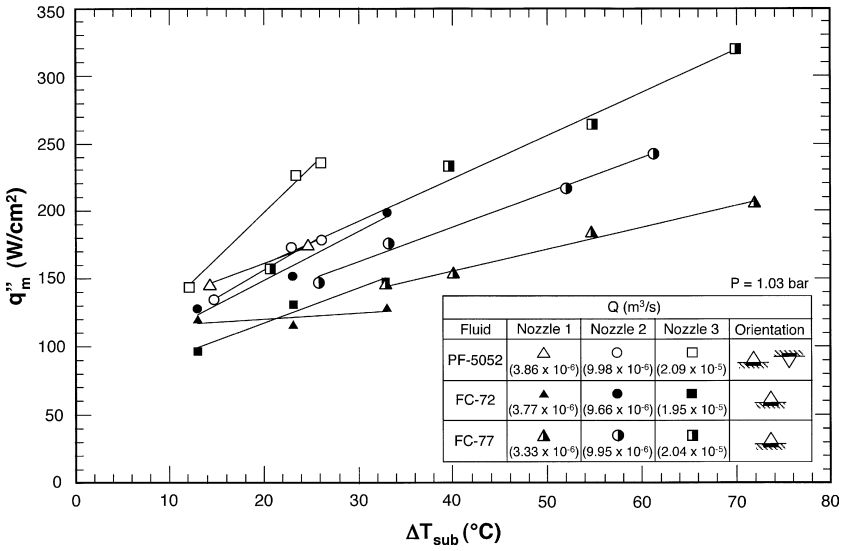

Fig. 6. Variation of CHF with subcooling for different nozzles, fluids, flow rates and orientations.

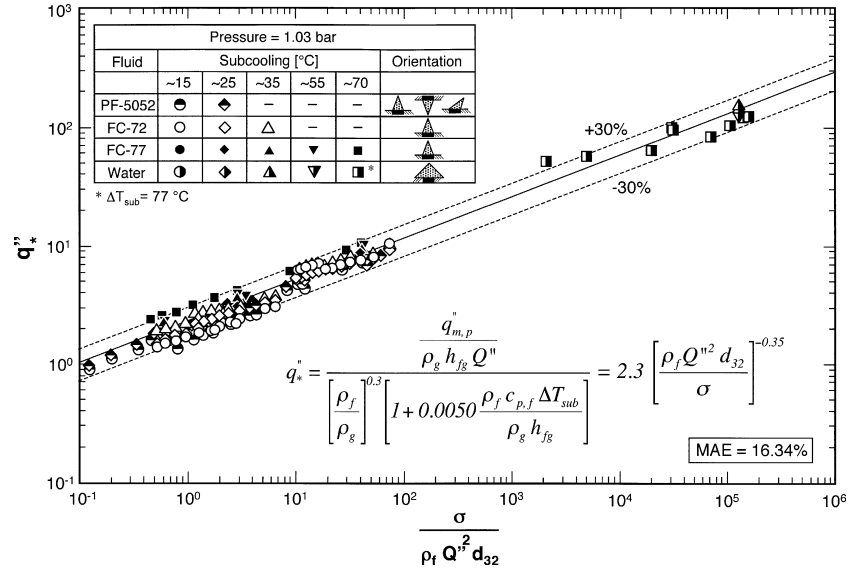

Fig. 7. Correlation of CHF data for different nozzles, fluids, flow rates, subcoolings and orientations.

of this correlation for different nozzles, fluids, flow rates and spray inclination.

Unfortunately, the range of subcooling for the data used to generate and later validate the CHF correlation was very limited. The new FC-77 data amassed in the present study is intended to correct this limitation by deriving a new correlation applicable to a broad range of subcooling. Incorporating the new FC-77 data quickly pointed out a more prominent effect of subcooling on CHF than predicted by Eq. (2). Using the entire CHF database given in Table 2 yielded the following new CHF correlation with a modified coefficient for the subcooling term:

$$\frac{q''_{m,p}}{\rho_g h_{fg} Q''} = 2.3\left(\frac{\rho_f}{\rho_g}\right)^{0.3}\left(\frac{\rho_f Q''^2 d_{32}}{\sigma}\right)^{-0.35}\left(1+0.0050\frac{\rho_f c_{p,f}\Delta T_{sub}}{\rho_g h_{fg}}\right). \quad (7)$$

Fig. 7 shows excellent predictive capability of Eq. (7) compared to the entire CHF database. Most of the data fall within ±30% of the correlation and the mean absolute error for the entire database is 16.34%. This comparison includes data for six different nozzles, four fluids (FC-72, FC-77, PF-5052 and water), upward-oriented, downward-oriented, and inclined sprays, and subcooling that ranges from 15 to 77 °C.

Table 2 provides detailed information about each CHF data point used in developing Eq. (7), including measured CHF, q''_m, local volumetric flux, Q'', mean volumetric flux, $\overline{Q}''$, Sauter mean diameter, d_{32}, and Weber number, *We* based on Q''.

4.3. Evaporation efficiency

Evaporation efficiency is another important spray performance parameter defined as the ratio of CHF to the maximum heat flux that can be removed by the spray.

$$\eta = \frac{q''_m}{\rho_f \overline{Q}''(c_{p,f}\Delta T_{sub} + h_{fg})} \times 100\%. \quad (8)$$

Fig. 8 shows η decreases monotonically with increasing Weber number. Weber number can be increased by increasing volumetric flux, increasing d_{32}, and/or decreasing surface tension. Increasing

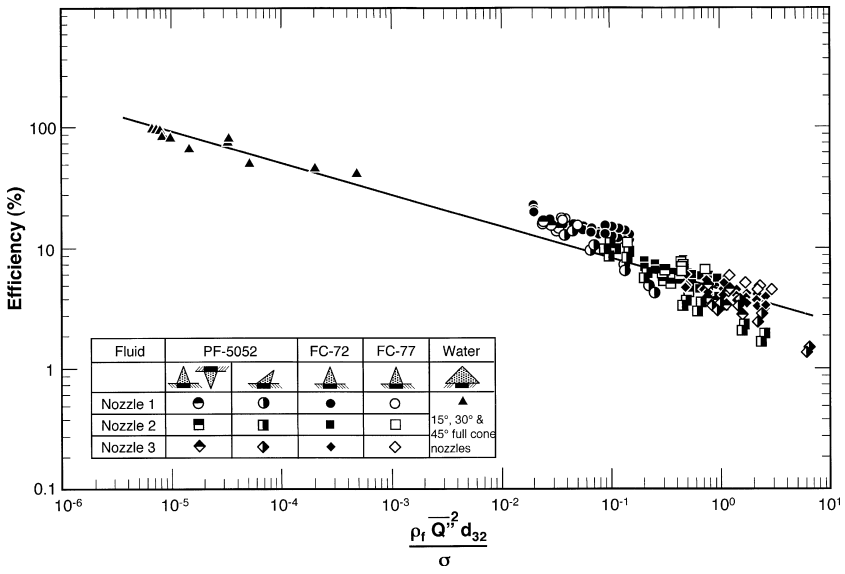

Fig. 8. Evaporation efficiency versus Weber number based on mean volumetric flux for PF 5052, FC-72, FC-77 and water.

flow rate increases liquid buildup on the test surface, reducing efficiency. Increasing d_{32} reduces liquid surface area to volume ratio, which also reduces spray efficiency. The high efficiency values for water in Fig. 8 are the result of both low volumetric flux of the water data and relatively high surface tension of water compared to the other fluids in the CHF database.

Interestingly, subcooling had no appreciable effect on evaporative efficiency. Efficiency for the same nozzle and flow rate but different subcoolings had fairly similar efficiency values.

5. Conclusions

This study examined the effects of subcooling on CHF in spray cooling. New spray CHF data were obtained using FC-77 as working fluid. The high boiling point (97 °C) of this fluid allowed testing over a fairly broad range of subcooling. The new data were combined with prior spray CHF data for different nozzles, fluids, flow rates, subcoolings and orientations. This database was used to modify an existing CHF correlation in pursuit of a more universal correlation. Key findings from this study can be summarized as follows.

1. Increasing subcooling delays the onset of boiling but decreases the slope of the nucleate boiling region of the spray boiling curve.
2. Increasing subcooling enhances CHF. This enhancement is relatively weak at low subcooling but becomes more pronounced for subcoolings in excess of 40 °C.
3. High subcooling is an effective means for dissipating high-heat fluxes. The present study yielded CHF values as high as 349 W/cm^2 and showed CHF can be improved by as much as 100% for the same fluid, nozzle, flow rate and orientation when subcooling is increased from 22 to 70 °C.
4. Aside from increased subcooling, CHF can be increased by increasing volumetric flux and/or decreasing droplet diameter.
5. A CHF correlation previously developed by Estes and Mudawar has shown accurate predictions for different nozzles, coolants, flow rates and spray orientations and relatively low subcoolings. The new FC-77 data show the subcooling parameter in this correlation must be modified for high levels of subcooling. A modified correlation is recommended that shows excellent predictive capability, evidenced by a mean absolute error of 16.34%.
6. Subcooling has no appreciable effect on evaporation efficiency. Efficiency is greater for low volumetric fluxes and nozzles that produce smaller droplets.

References

[1] I. Mudawar, Assessment of high-heat-flux thermal management schemes, IEEE Trans. – Comp. Packag. Technol. 24 (2001) 122–141.
[2] S. Toda, A study in mist cooling (1st report: investigation of mist cooling), Trans. Jpn. Soc. Mech. Eng. 38 (1972) 581–588.
[3] I. Mudawar, W.S. Valentine, Determination of the local quench curve for spray-cooled metallic surfaces, J. Heat Treating 7 (1989) 107–121.
[4] M. Monde, Critical heat flux in saturated forced convection boiling on a heated disk with impinging droplets, Trans. Jpn. Soc. Mech. Eng. 8 (1979) 54–64.
[5] S. Toda, H. Uchida, Study of liquid film cooling with evaporation and boiling, Trans. Jpn. Soc. Mech. Eng. 2 (1973) 44–62.
[6] K.A. Estes, I. Mudawar, Correlation of Sauter mean diameter and critical heat flux for spray cooling of small surfaces, Int. J. Heat Mass Transfer 38 (1995) 2985–2996.
[7] I. Mudawar, K.A. Estes, Optimizing and predicting CHF in spray cooling of a square surface, J. Heat Transfer 118 (1996) 672–680.
[8] C.S.K. Cho, K. Wu, Comparison of burnout characteristics in jet impingement cooling and spray cooling, in: Proceedings of National Heat Transfer Conference, vol. 1, Houston, Texas, 1988, pp. 561–567.
[9] R.-H. Chen, L.C. Chow, J.E. Navedo, Effects of spray characteristics on critical heat flux in subcooled water spray cooling, Int. J. Heat Mass Transfer 45 (2002) 4033–4043.
[10] J.R. Rybicki, I. Mudawar, Single-phase and two-phase cooling characteristics of upward-facing and downward-facing sprays, Int. J. Heat Mass Transfer 49 (2006) 5–16.
[11] M. Visaria, I. Mudawar, Theoretical and experimental study of the effects of spray inclination on two-phase spray cooling and critical heat flux, Int. J. Heat Mass Transfer 51 (2008) 2398–2410.
[12] M. Visaria, I. Mudawar, A systematic approach to predicting critical heat flux for inclined sprays, J. Heat Transfer J. Electron. Packaging 129 (2007) 452–459.
[13] L. Lin, R. Ponnappan, Heat transfer characteristics of spray cooling in a closed loop, Int. J. Heat Mass Transfer 46 (2003) 3737–3746.
[14] A.G. Pautsch, T.A. Shedd, Spray impingement cooling with single- and multiple-nozzle arrays. Part I: heat transfer data using FC-72, Int. J. Heat Mass Transfer 48 (2005) 3167–3175.
[15] M.S. Sehmbey, M.R. Pais, L.C. Chow, Effect of surface material properties and surface characteristics in evaporative spray cooling, J. Thermophys. Heat Transfer 6 (1992) 505–512.
[16] E.A. Silk, J. Kim, K. Kiger, Effect of spray cooling trajectory on heat flux for a straight finned enhanced surface, in: Proceedings of National Heat Transfer Summer Conference, Paper HT2005-72634, San francisco, California, 2005.
[17] B.Q. Li, T. Cader, J. Schwarzkopf, K. Okamoto, B. Ramaprian, Spray angle effect during spray cooling of microelectronics: experimental measurements and comparison with inverse calculations, Appl. Therm. Eng. 26 (2006) 1788–1795.